JOURNAL OF CATALYSIS 38, 402–417 (1975)

A Study of the Kinetics and Mechanism of the Decomposition of Formic Acid on Carburized and Graphitized Ni(110) Using AES, LEED and Flash Desorption

J. McCARTY[1] AND R. J. MADIX[2]

Department of Chemical Engineering, Stanford University, Stanford, California 94305

Received November 13, 1974

The decomposition of formic acid on Ni(110)(2 × 1)C, Ni(110)(4 × 5)C *surface* carbides and Ni(110)–graphite, an overlayer of graphitic carbon, was studied using Auger electron spectroscopy (AES) and low energy electron diffraction (LEED) to characterize the nature of the surfaces. On the carbide surface the autocatalytic mechanism observed previously for clean Ni(110) was suppressed, and the decomposition occurred via a multicentered ring transition state involving the adsorbed intermediate HCOO. The first-order rate constant for this step was $10^{12} \exp\{-25{,}000/RT\}$ s^{-1}. The reaction probability was unity for the carbide surfaces as on the clean surface, and adsorption of formic acid was dissociative, producing adsorbed hydrogen atoms and HCOO(a). The selectivity of the carbide surface for hydrogen production was 10 times that of the clean surface, due to the formation of a different reaction intermediate. In addition, the graphitic overlayer reduced the probability of decomposition on the surface by at least an order of magnitude; the Ni(110)–graphite surface was essentially inactive for the decomposition.

INTRODUCTION

Auger electron spectroscopy (AES), low energy electron diffraction (LEED) and flash desorption spectroscopy (FDS) allow one to study chemical reactions on surface compounds of known composition and structure. The purpose of this work was to illustrate the usefulness of studies of this nature and their relevance to more conventional studies in catalysis, and to clarify many features of the decomposition of formic acid that remain points of controversy in the literature.

Recent work by Inglis and Taylor (*1*) showed the selectivity of formic acid decomposition on freshly deposited films to be sensitive to contamination. They observed that the product ratio for the dehydrogenation and dehydration reactions, respectively, was 2.5 on fresh nickel films. After several experimental runs the activity decreased and the CO_2/CO ratio increased to about 10, the value typically seen on nickel powders, wires, foils, etc. (*2,3*). The decreased activity was attributed to contamination of unknown origin. Our previous results (*4*) for the decomposition of formic acid adsorbed on clean Ni(110) showed an even lower CO_2/CO product ratio, 1.0, than the results of Inglis and Taylor. The Ni(110) surface was cleaned by sputtering; the total impurity concentration at the surface was measured by Auger electron spectroscopy and found to be less than 5×10^{13} atoms/cm^2. Apparently the CO_2/CO product ratio is low on clean nickel, implying that nickel catalysts producing a high CO_2/CO product ratio were contaminated.

Duell and Robertson (*5,6*) reported that

[1] In partial fulfillment of the requirements for the PhD degree.

[2] To whom inquiries should be addressed.

the reaction probability, P, on nickel wires at 700°K drastically decreased from 1 to 10^{-5} after several minutes exposure to 2×10^{-4} Torr of formic acid. High activity, $P = 1$, was initiated and often restored by flash heating a nickel wire to 1600°K. The loss of activity was attributed to either the depletion of active sites such as vacancies or contamination with carbon.

Our goal in this study was to determine if surface carbon significantly altered the activity and selectivity of nickel for the decomposition of formic acid. LEED and AES were used to identify the structure and relative coverage of carbide and graphitic surface layers on a nickel (110) single crystal. The fine structure of the carbon Auger spectra was used to identify the carbide and graphite forms of surface carbon (*7–10*). The (2×1)-C and (4×5)-C carbide structures (*11,12*) and the segmented ring pattern characteristic of graphite (*11,12,13*) were identified by LEED. The decomposition of adsorbed formic acid was studied using the flash desorption technique, and the results were compared with the previously reported results for decomposition on clean Ni(110) (*4,14*). A portion of the results reported here were previously published in a short communication (*15*).

EXPERIMENTAL METHODS

The apparatus and techniques used in this investigation for Auger spectroscopy and flash desorption have been previously described (*4*). The apparatus is briefly described again here as follows. The experiments were conducted in a stainless steel ultrahigh vacuum chamber which was operated below 10^{-9} Torr during flash desorption. The system was equipped with four-grid LEED–Auger electron optics and a quadrupole mass spectrometer. The thin Ni(110) crystal could be cooled below 175°K with liquid nitrogen, or heated above 750°K by radiation from a tungsten filament. The heating rate could be varied from 0.1 to 25°K/s and was typically 10 to 15°K/s. Gases were introduced to the sample through a hypodermic syringe directed at the crystal surface or through a variable leak valve attached to the chamber wall. During flash desorption the partial pressures of desorbing gases were measured by the mass spectrometer as a function of the sample temperature (*16*).

By using the doser adsorption from the residual gas in the vacuum chamber was virtually eliminated. Because the pumping speed for HCOOH, H_2O, CO, CO_2 and H_2 was greater than 1000 liters/sec, the background pressure during dosing was kept below 10^{-9} Torr while the effective pressure at the surface of the sample was two orders of magnitude higher. The extent of background adsorption was determined by dosing with the sample out of alignment with the doser syringe. Background adsorption contributed only minimally to the flash desorption peaks for short exposure times. The doser exposure was calibrated by comparing CO doser adsorption to adsorption of CO when introduced into the vacuum chamber via a variable leak valve.

The doser exposure of HCOOH was determined from the conductivity of HCOOH through the doser syringe relative to CO. The shape of the beam of gas flowing away from the doser was assumed to be independent of the mass of the gas molecules. The net conductivity and hence the total flux of a gas passing through the doser was assumed to vary with the inverse of the square root of mass. Thus the HCOOH doser exposure was taken as $(28/46)^{1/2}$ or 78% of the calibrated CO doser exposure.

Surface carbon was deposited by cracking ethylene. The temperature of the sample during deposition determined whether the carbide or graphite surface was formed (*12*). Two LEED structures of the carbide surface were identified in agreement with Pitkethley (*12*) and Ertl

(*11*); the (2 × 1)-C structure was formed by deposition at 500 to 550°K and the (4 × 5)-C structure was formed by deposition at 575 to 625°K in 10^{-7} Torr C_2H_4. The carbon coverage of the (4 × 5)-C surface deposited at 600 ± 25°K following saturation exposure to ethylene was defined as 1.0 C_{et}.

Figure 1 shows the Auger carbon spectra for the carbide and graphite surfaces. Figure 1a shows a typical carbon KVV (270 eV) Auger spectrum of the Ni(110) surface after an ethylene exposure of 120 Langmuir at 600°K. Further ethylene exposure did not increase the carbon Auger signal strength. The presence of Auger peaks at 258 and 249 eV in the fine structure just below the strong 270 eV peak in Fig. 1a was characteristic of a carbide surface layer. The carbide designation was based on the work of Haas *et al.* (*9,10*) and Grant and Haas (*17*) who compared the carbon Auger fine structures of graphite, refractory metal carbides and adsorbed CO. This fine structure is in excellent agreement with that observed for surface carbide on Ni(111) by Dalmai-Imelik *et al.* (*8*).

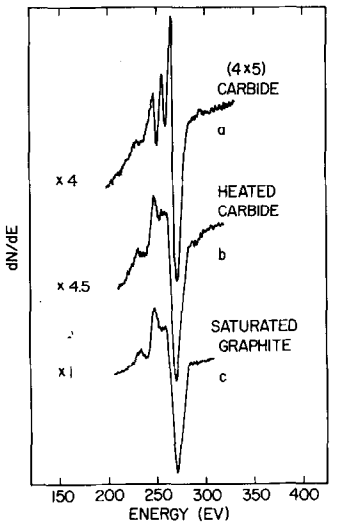

FIG. 1. Carbon KVV Auger spectra of the carbide and graphite forms of surface carbon on Ni(110). (a) Auger spectrum of a (4 × 5)-C saturated carbide surface formed at 550°K by a doser exposure of C_2H_4 equivalent to 200 Langmuir. (b) Graphite Auger spectrum formed by heating a saturated carbide layer to 775°K for 15 s. (c) Auger spectrum of a saturated graphite surface formed at 725°K by a doser exposure of C_2H_4 equivalent to 180 Langmuir. The energy of the incident electron beam was 2.0 keV and the modulation voltage was 2.0 V_{rms}, except (b) which had 3.0 V_{rms} modulation voltage. The indication of the relative signal magnitude has been corrected for the difference in modulation voltage, by presuming the dN/dE signal was proportional to the square of the modulation voltage.

The carbide surface was unstable above 700°K; heating the carbide layer to 800°K or cracking ethylene at 800°K produced surface graphite. Figure 1b shows the result of heating the carbide surface in Fig. 1a to 775°K; the surface carbide was transformed into surface graphite without a significant loss of surface carbon. The AES fine structure of Fig. 1b and c was characteristic of graphite. The surface represented by the AES of Fig. 1b adsorbed hydrogen and decomposed formic acid explosively (*4*), indicating the presence of clean nickel; the graphite apparently formed islands consistent with the higher two-dimensional density of the basal plane of graphite as observed previously by Ertl (*11*) and Pitkethly (*12*). Continuous exposure of the Ni(110) to ethylene at 800°K produced a graphite layer represented by Fig. 1c. The carbon coverage reached a limiting value at an ethylene exposure less than 180 Langmuir, indicating that graphite was not continually grown on the surface.

The graphite surface was formed at temperatures above 675°K. The graphite layer showed LEED patterns characteristic of the basal plane of crystalline graphite as observed by Ertl (*11*) and Pitkethly (*12*). At saturation exposure to 10^{-7} Torr ethylene the carbon coverage of the graphite surface approached 3.8×10^{15} atoms/cm^2, the surface density of a monolayer of graphite. Based on AES measurements of the carbide coverage relative to the graphite coverage, the coverage of surface

carbon in the (2 × 1) and (4 × 5) carbide surfaces was 9×10^{14} atoms/cm^2 (*18*).

RESULTS

A. HCOOH and DCOOH Decomposition of the Carbide Surfaces

The presence of carbon in the carbide form on Ni(110) decreased the overall formic acid decomposition rate and eliminated the kinetic explosion characteristic of decomposition on the *clean* surface. Room temperature adsorption of HCOOH (*4*) and DCOOH (*14*) on the clean surface produced very narrow CO_2 and H_2 or D_2 flash desorption curves characteristic of an autocatalytic decomposition. The very narrow CO_2 and H_2 flash peaks following adsorption of HCOOH at 315°K were reproducible for carbon coverage up to a tenth of a monolayer (0.1 C_{et}). In a series of experiments the concentration of surface carbon was incrementally increased by mixing a small amount of carburizing contaminant, acetic acid, with the formic acid. The narrow peaks ($\Delta T_{1/2} = 6$°K) initially broadened; and as $\Delta T_{1/2}$ approached 20°K with subsequent flashes, the temperature at maximum rate gradually shifted from 388°K to a maximum of 438°K at 0.9 C_{et} carbide coverage. In Fig. 2 the CO_2 flash curves produced by formic acid decomposition on the clean and the saturated carbide (1.0 C_{et}) surfaces are compared for the same formic acid exposure, 4×10^{14} molecules/cm^2, at 315°K. These flash curves represent nearly equal total coverage.

The initial sticking probability and the maximum coverage for room temperature adsorption of formic acid on the saturated carbide surface apparently was not effected by the presence of the carbon atoms. The initial sticking probability on the (4 × 5)-C surface was unity as on clean Ni(110) (*4*). The maximum coverage of decomposition intermediate observed for

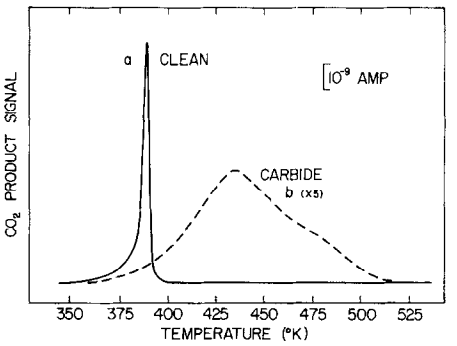

FIG. 2. CO_2 flash desorption for HCOOH decomposition on the clean and the (4 × 5) carbide surfaces. HCOOH exposure for both curves on (a) the clean surface and (b) the saturated carbide surface was 2400 μs or 4×10^{14} molecules/cm^2. The heating rate at 425°K was 8°K/s.

the (4 × 5)-C surface following HCOOH exposure at room temperature was nearly the same as for the clean surface, $3 \pm 1 \times 10^{14}$ vs $4 \pm 1 \times 10^{14}$ molecules/cm^2, respectively.

The CO_2 flash curves produced by formic acid decomposition following adsorption on the carbide surface indicated the reaction intermediate had two binding states. Since CO_2 did not adsorb on this surface, it can be safely assumed that the evolution of product CO_2 was not desorption limited. Figures 3 and 4 show a series of CO_2 flash curves for increasing HCOOH and DCOOH exposure, respectively, at 310°K on saturated carbide surfaces. Two states, designated β_1 and β_2 in Figs. 3 and 4, appeared with maximum rates at 438 ± 10 and 473 ± 10°K, respectively, for HCOOH. Similar states appeared at 448 ± 10 and 473 ± 10°K, respectively, for DCOOH. The β_2 states were filled first for low exposures of both DCOOH and HCOOH; but as the exposure increased, the β_1 states appeared. As the total coverage reached a saturation value of $3 \pm 1 \times 10^{14}$ molecules/cm^2 for both DCOOH and HCOOH, the β_1:β_2 coverage ratio approached 1 : 1.

The activation energy and frequency factor for decomposition was found to be

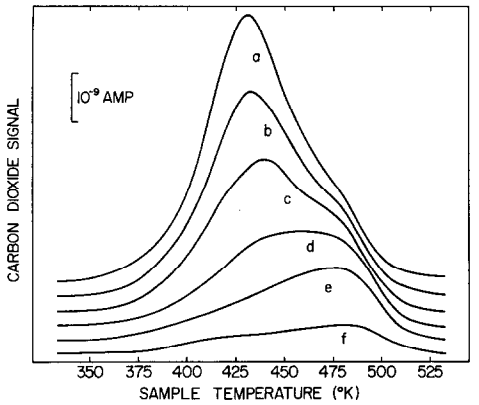

FIG. 3. CO_2 desorption for HCOOH decomposition on the saturated (4 × 5) carbide surface following adsorption at 310°K. The HCOOH doser exposures were ($\times 10^{14}$ molecules cm^{-2}) (a) 5.6, (b) 3.75, (c) 1.82, (d) 1.26, (e) 0.56 and (f) 0.14. 1.75×10^{11} molecules $cm^{-2} = 1$ μs exposure. The heating rate was 8°K s^{-1}.

28 ± 3 kcal/g-mole and $10^{13\pm2}$ s^{-1} for the β_1 state and 16 ± 3 kcal/g-mole and $10^{6\pm2}$ s^{-1} for the β_2 state. These values were determined by fitting first-order rate models to the data by trial and error. The uncertainty of these values reflects the reproducibility of the data for different saturated carbide surfaces. A more complete analysis of the CO_2 flash decomposition curves is discussed below.

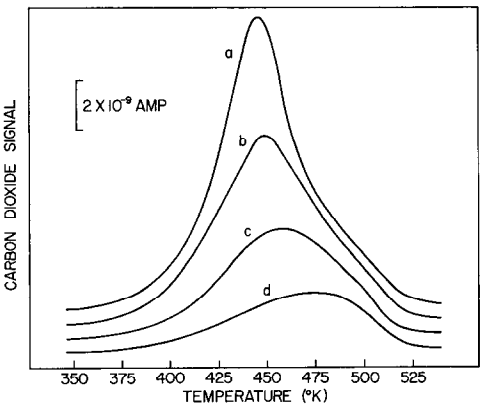

FIG. 4. CO_2 desorption for DCOOH decomposition on a saturated (4 × 5) carbide surface following adsorption at 310°K. The DCOOH exposures were ($\times 10^{14}$ molecules/cm^{-2}) (a) 5.6, (b) 2.8, (c) 1.4 and (d) 0.7. 1 μs = 0.8×10^{11} molecules cm^{-2}. The heating rate was 11°K s^{-1}.

The decomposition of HCOOH and DCOOH on the (4 × 5)-C surface indicated that the predominant intermediate was a species with the composition HCOO or DCOO. H_2 desorbed in curves nearly identical to the CO_2 desorption curves following HCOOH adsorption at 310°K. The ratio of H_2 to CO_2 desorbed was 0.6 ± 0.2 in contrast to the value of 1.0 ± 0.2 found for decomposition on the clean surface. As on the clean surface (*4*) H_2 was not detected in either the β_1 or β_2 states following DCOOH adsorption at 310°K. The D_2 desorption curves were indistinguishable from the CO_2 curves and the D_2 to CO_2 ratio was 0.5 ± 0.2. Flash desorption of D_2O, HDO, and H_2O was not detectable following DCOOH adsorption at 310°K. Evidently the acid hydrogen desorbed immediately following adsorption of formic acid at these temperatures.

The (4 × 5) carbide surface was 10 times more selective toward dehydrogenation, i.e., decomposition into H_2 and CO_2, than the clean Ni(110) surface. The ratio of CO_2:CO products following room temperature HCOOH adsorption on the clean surface was 0.3:1 at low coverage increasing to 1:1 at saturation. On the (4 × 5)-C surface this ratio was 3 ± 1:1 at lower coverage and 10 ± 5:1 at saturation. The mass spectrometer ionizer cracked CO_2 and produced CO^+ ions with 23% of the CO_2^+ signal strength. At high coverage the mass 28 signal from desorbing CO_2 was larger than the mass 28 signal from desorbing CO, and created the large uncertainty in the actual amount of CO desorbed. Figure 5 shows the CO and CO_2 contributions to the total CO^+ signal for DCOOH decomposition on the (2 × 1)-C surface for both high and low exposure at 310°K. The net CO coverage of Fig. 5a was 1.6×10^{13} molecules/cm^2 following a DCOOH exposure of approximately 9×10^{14} molecules/cm^2. The net CO coverage of Fig. 5b was 0.7×10^{13} molecules/cm^2 following a

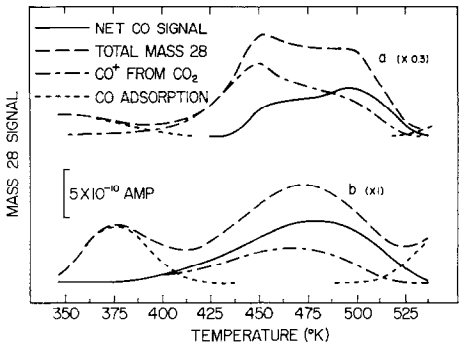

FIG. 5. CO desorption for DCOOH decomposition on the (2 × 1) carbide Surface. (--) Total mass spectrometer signal at 28 AMU. (—) CO^+ contribution from desorbed CO_2. (---) CO desorption attributed to adsorbed CO for $T < 425$°K or oxidation of the carbide layer for $T > 500$°K. (–) Net CO desorption due to the decomposition of DCOOH. (a) The net CO coverage was 1.6×10^{13} molecules/cm^2 after an exposure of 8.5×10^{14} molecules/cm^2. (b) The net CO coverage was 0.7×10^{13} molecules/cm^2 after an exposure of 0.4×10^{14} molecules/cm^2. The adsorption temperature was 310°K for both (a) and (b); the heating rate for both was 11°K/s.

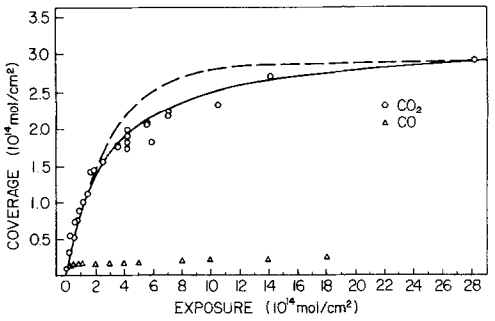

FIG. 6. Product coverage vs HCOOH exposure to the (4 × 5)-C surface following adsorption at 310°K. (--) $S \propto (1 - \theta)$. (–) $S \propto (1 - \theta)^2$. Heating rate 8°K s^{-1}.

DCOOH exposure of approximately 4×10^{13} molecules/cm^2. The CO from formic acid decomposition desorbed at a higher temperature ($T_p = 476 \pm 10$°K) than CO desorption from *adsorbed* CO ($T_p = 360 \pm 10$°K).

The peak temperature (T_p) of the CO desorption flash curve from formic acid decomposition was near the T_p observed for the β_2-CO_2/HCOOH flask peak. Apparently CO and β_2-CO_2 were produced from the same reaction steps or from parallel reaction steps with similar rate constants. Unfortunately the CO_2 cracking fraction contribution to the CO^+ signal obscured the net CO desorption rate, and definitive comparison of the CO and β_2 CO_2/HCOOH peak shapes was not possible. The CO/HCOOH state was not desorption limited. Occasionally a small amount of CO, always less than 1×10^{13} molecules/cm^2, appeared at 365°K (see Fig. 5) due to CO adsorption from the residual gas in the vacuum system.

The initial sticking probability, S, of formic acid on the (4 × 5)-C and (2 × 1)-C surfaces at 315°K was near unity. In Fig. 6 the coverage of CO_2 and CO (corrected by subtracting the CO^+ contribution from CO_2) is plotted against exposure for the (4 × 5)-C surface. The doser exposure was calibrated as discussed above by comparing the clean surface adsorption of CO introduced through the doser against the adsorption from CO background pressure in the chamber. Saturation coverage was $3 \pm 1 \times 10^{14}$ molecules/cm^2 on both the (4 × 5) and (2 × 1) carbide surfaces. Figure 6 also shows the adsorption curves expected for $(1 - \theta)$ and $(1 - \theta)^2$ adsorption isotherms. Both curves in Fig. 6 were adjusted to produce the observed initial sticking probability and saturation coverage. The actual adsorption isotherm closely followed the $(1 - \theta)^2$ curve implying that two adjacent sites were required for adsorption of formic acid at 315°K.

Although H_2 was not detected following DCOOH adsorption on the (4 × 5)-C surface at 310°K, H_2 desorbed in a broad peak at 285 ± 10°K following DCOOH adsorption at 175°K; the position and shape of the D_2, CO_2 and CO peaks following DCOOH adsorption did not change. The amount of H_2 produced from DCOOH decomposition was substantially greater than the maximum coverage from H_2 adsorption; the ratio of H_2 to D_2

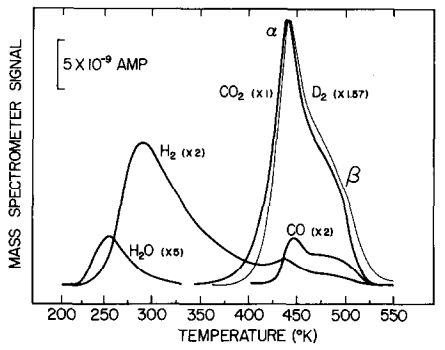

FIG. 7. Product desorption curves for DCOOH decomposition on the (2 × 1) carbide surface. The DCOOH doser exposure was 3200 μs or 5.6×10^{14} molecules/cm^2 at a surface temperature of 200°K. The heating rate varied from 15°K/s at 200°K to 10°K/s at 500°K.

flashed following the low temperature adsorption was 1.0 ± 0.2. A small amount of H_2O, about 4% of the coverage at saturation H_2O exposure, was detected at 255 ± 10°K following a 2 Langmuir DCOOH exposure at 210°K. This represented about 10% of the CO_2 coverage and was comparable to the amount of CO product. HDO and D_2O were not detected following adsorption on the cold surface. Figure 7 shows the H_2, H_2O, D_2, CO, and CO_2 flash curves following a 2 Langmuir DCOOH exposure to the (2 × 1)-C surface at 200°K. The CO curve represents the net CO desorption rate for DCOOH decomposition. A product signal of 10^{-8} A in Fig. 7 for H_2, H_2O, CO_2, D_2 and CO represented desorption rates of approximately 4, 12, 4, 3, and 4×10^{13} molecules/cm^2/s, respectively. Thus the size of the H_2, H_2O, CO and D_2 peaks were indicative of their actual coverage and the CO_2 peak was plotted approximately half as large as its actual relative magnitude.

B. Formic Acid Decomposition on the Graphite Surface

The (4 × 5)-C structure remained stable during a series of flashing cycles provided the maximum flash temperature was held below 550°K. The oxygen Auger signal increased to levels seen following decomposition on the clean surface and upon heating to 775°K, CO peaks at 655 and 775°K were produced. These CO peaks have been attributed to the reaction of oxygen with carbide and graphite forms, respectively, of surface carbon (*4,19*). Flash heating the carbide surface to 775°K once or twice was all that was necessary to restore the sharp CO_2/H_2 peaks characteristic of decomposition on the clean surface. The carbon Auger current after one such flash usually decreased only slightly, characteristic of nearly constant carbon *coverage*. Some of the carbide reacted with the adsorbed oxygen to produce CO and the remainder formed graphite "islands" over the nickel surface as reported elsewhere (*18*).

The saturated graphite surface produced only small amounts of CO and CO_2 decomposition products. A 3 Langmuir DCOOH exposure at 310°K produced $1.5 \pm 0.5 \times 10^{13}$ molecules/cm^2 of both CO and CO_2 which desorbed into broad peaks centered at 430 ± 10°K ($\Delta T_{1/2} =$ 80°K). Both the clean and the saturated carbide surfaces produced 10 times this amount of product under the same adsorption conditions.

C. Summary of Results

Table 1 summarizes the results obtained for formic acid decomposition on the clean, carbide, and graphite surfaces. The notation, β-CO/DCOOH, refers to the β state of the CO desorption peak following adsorption of DCOOH. Whenever possible, the desorption activation energy, $E_{\Delta T_{1/2}}$, and frequency factor, A, of a state based on the peak shape or a desorption model are included in Table 1. E^* was calculated from the peak temperature of each state assuming a first order slow step with a frequency factor of 10^{13} s^{-1}. In other words, E^* represents the binding activation energy for a hypothetical first-

TABLE 1
FORMIC ACID DECOMPOSITION ON CLEAN, CARBURIZED, AND GRAPHITIZED Ni(110)

	State	T_{ads} (°K)[a]	Surface	N_s ($\times 10^{14}$)[b]	S_0[c]	T_p (°K)[d]	$\Delta T_{1/2}$ (°K)[e]	$E_{\Delta T}$[f]	$\log_{10} A$[f]	E^*[g]
β_1	CO_2/HCOOH	200–310	Carbide	3 ± 1	0.7	438 ± 10	—	25.5 ± 2	12.5 ± 1	26.4
$\beta_{2,3}$	CO_2/HCOOH[h]	200–310	Carbide	3 ± 1	0.7	473 ± 10	—	26 ± 2[h]	11.5 ± 1[h]	28.9
β_1	CO_2/DCOOH	200–310	Carbide	3 ± 1	0.7	448 ± 10	—	26 ± 2	12.6 ± 1	27.0
$\beta_{2,3}$	CO_2/DCOOH[h]	200–310	Carbide	3 ± 1	0.7	473 ± 10	—	26 ± 2[h]	11.5 ± 1[h]	28.9
	CO_2/DCOOH	175–310	Graphite	0.2	0.05	430 ± 20	—	—	—	26.0
	$H_2 + CO_2$/HCOOH	310	Clean	2	1	388	6.5	26.1 ± .5	15.4 ± .3	23.3
	$D_2 + CO_2$/DCOOH	310	Clean	2	1	397	6.5	26.6[i]	15.1[i]	23.9
	CO/HCOOH	200–310	Carbide	0.3	0.3	460 ± 20	—	—	—	27.5
	CO/DCOOH	200–310	Carbide	0.3	0.3	460 ± 20	—	—	—	27.5
	CO/DCOOH	175–310	Graphite	0.4	0.1	430 ± 20	—	—	—	26.0
α_2	CO/HCOOH	225–310	Clean	1.5	0.5	438	33	32[i]	15.9[i]	26.4
α_1	CO/HCOOH	225–310	Clean	0.5	0.5	375 + 5	—	—	—	22.4
	H_2/DCOOH	200–225	Carbide	1.3	0.9	288 ± 5	45[j]	13[k]	4[k]	16.0
	D_2/HCOOD	200	Clean	<0.2	—	—	—	—	—	—
	H_2O/DCOOH	200–225	Carbide	0.1	0.1	255	28[j]	11.5[k]	10[k]	14.9
	D_2O/HCOOD	200	Clean	—	>0.9	315	—	—	—	18.4
	H_2O/DCOOH	200	Clean	—	>0.9	330	—	—	—	19.3

[a] T_{ads} is the adsorption temperature.
[b] N_s represents the maximum number of adsorbed formic acid molecules which contributed to the observed product flash peak or peaks (10^{14} molecules/cm^2).
[c] S_0 represents the initial fraction of the incident formic acid molecules which eventually contributed to the observed product flash peak or peaks for adsorption at 310°K.
[d] T_p is the peak temperature for a heating rate of 10°K/s.
[e] $\Delta T_{1/2}$ is the full width at one-half the maximum desorption rate.
[f] $E_{\Delta T}$ and A represent the activation energy (kcal/g-mole) and frequency factor (s^{-1}) of the surface reaction or desorption step limiting the evolution of the product gas. Except where noted, $E_{\Delta T}$ and A were determined from the calculated curves best describing the decomposition.
[g] E^* is the activation energy (kcal/g-mole) calculated for a single first-order rate-limiting step from T_p assuming $\log_{10} A \equiv 13$.
[h] The β_2 and β_3 states are combined together, $E_{\Delta T}$ and A of both states fall within the specified range.
[i] Calculated from the shift in T_p with variation in the heating rate (*14*).
[j] Extrapolated from the leading edge of the desorption curve assuming a first-order rate-limiting step.
[k] Calculated for a first-order desorption peak having the same $\Delta T_{1/2}$.
[l] In all cases observed the H_2/CO_2 ratio was 1:2.

order reaction step with $A \equiv 10^{13}$ s^{-1} which has the same peak temperature as the observed product peak. This activation energy provides a relative value for those states for which peak shape analysis was not meaningful.

DISCUSSION

A. Comparison with Earlier Work

The results presented above clearly demonstrate that carbon contamination as a carbide layer decreased the activity and increased the selectivity for CO_2 of formic acid decomposition on Ni(110). Carbide surfaces formed by saturation exposure to ethylene were substantially less active than "clean" surfaces. A reasonable measure of relative activity with the flash desorption technique, for example, is the peak temperature. The peak temperature of decomposition on the surface carbide, 440°K, was 50°K higher than that for the clean surface. When extrapolated at 26.6 kcal/g-mole from 390 to 440°K, the de-

composition rate on the clean surface was two orders of magnitude greater than decomposition on the carbide surface for the same initial coverage. Furthermore, defining selectivity as the CO_2 to CO product ratio, the saturated carbide surface selectivity was 10 whereas the clean surface selectivity was 1.0—an order of magnitude lower.

The presence of surface compounds during the decomposition of HCOOH may explain observations of previous workers. For example, the formation of a carbide layer may explain the decreased activity and increased CO_2/CO selectivity observed by Inglis and Taylor (*1*) after several formic acid decompositions runs on evaporated nickel films. Several possible sources of surface carbon are diffusion of bulk carbon to the surface of the films, disproportionation of product CO (*20*), or small amounts of carburizing impurities such as acetic acid or methanol in the formic acid. Our results on Ni(110) demonstrated that small amounts of acetic acid impurity can produce a carbide layer. Both the carbide surface formed by the acetic acid and the saturated carbide surface formed by cracking ethylene were stable at temperatures up to 600°K, the maximum temperature used by Taylor *et al.* Above 600°K the carbide surface transformed into the inactive graphitic form.

Formation of a graphite layer could also have caused the loss of "superactivity" reported by Duell and Robertson (*5,6*) for formic acid decomposition on nickel wires. They observed that decomposition probability of HCOOH at 700 to 1000°K and 10^{-4} to 10^{-3} Torr was initially near unity for wires previously flashed to 1600°K. However, with prolonged formic acid exposure the reaction probability decreased several orders of magnitude. Our results show that a layer of graphite on Ni(110) was essentially inactive to formic acid decomposition. The most significant property of a graphite layer formed by saturation ethylene exposure at 750°K was the ability to adsorb and desorb formic acid at low temperature. The desorption of formic acid from the saturated graphite surface will be reported elsewhere. The flash desorption of formic acid from the graphite surface suggested that the residence time of a single adsorbed formic acid molecule was less than 100 ms even at 190°K. One might therefore expect a very short residence time, perhaps of the order 10^{-8} s, on a graphite layer at the temperatures used by Robertson *et al.* As a result the decomposition probability on graphitized nickel wires should be very low since an incident molecule could desorb before finding an active site.

A graphite layer on nickel will not dissolve into the bulk at low temperatures, and indeed many precipitate from bulk nickel if the concentration of dissolved carbon is sufficiently high. Blakely *et al.* (*21*) and Shelton *et al.* (*22*) have shown for Ni(100) and Ni(111) and Coad and Rivière (*7*) have shown for polycrystalline nickel that graphite will segregate to the nickel surface at 100°K with a bulk carbon concentration of 0.3 atomic percent. Coad and Rivière (*7*) have also shown that a carbide layer will precipitate from dissolved carbon in polycrystalline nickel at temperatures in the vicinity of 600°K. Thus, in order to predict the activity and selectivity of a nickel surface, one must account for the possible formation of carbide or graphite layers due to surface segregation of dissolved carbon as well as deposition from the gas phase.

B. Formic Acid Decomposition on the Carbide Surface

Our results indicated that on a monolayer of carburized Ni(110) formic acid (written here as DCOOH in order to distinguish between the oxygen and carbon bound hydrogen atoms) dissociatively adsorbed to form a stable adsorbed species, DCOO, and hydrogen which desorbed

immediately at room temperature. In addition a *small* amount of formic acid reacted to form H_2O which, like H_2, readily desorbed at room temperature, presumably leaving adsorbed DCO and DCOO fragments behind. Above 400°K DCOO decomposed into D_2 and CO_2 exhibiting at least two and perhaps three decomposition peaks. DCO apparently decomposed into D_2 and CO simultaneously with the DCOO decomposition. These results suggested the following reaction scheme for formic acid decomposition between 220 and 500°K.

Adsorption	DCOOH(g)	$\rightarrow$ DCOOH(a),	(1)
Dissociation into DCOO	DCOOH(a)	$\rightarrow$ DCOO(a) + H(a),	(2a)
	2H(a)	$\rightarrow$ H_2(g),	
	or 2DCOOH(a)	$\rightarrow$ 2DCOO(a) + H_2(g),	(2b)
Dissociation into DCO	DCOOH(a)	$\xrightarrow{\sigma}$ DCO(a) + OH(a),	(3a)
	H(a) + OH(a)	$\rightarrow$ H_2O(a) $\rightarrow$ H_2O(g),	
	or 2DCOOH(a)	$\xrightarrow{\sigma}$ DCO(a) + DCOO(a) + H_2O(a),	(3b)
	H_2O(a)	$\rightarrow$ H_2O(g),	
Decomposition	β_1 DCOO(a)	$\rightarrow$ D(a) + CO_2(g),	(4)
	β_2 DCOO(a)	$\rightarrow$ D(a) + CO_2(g),	
	DCO(a)	$\rightarrow$ D(a) + CO(a),	(5)
Desorption	2D(a)	$\rightarrow$ D_2(g),	(6)
	CO(a)	$\rightarrow$ CO(g).	(7)

The overall selectivity of the decomposition was determined by the competition between the dissociation steps (2) and (3). Since D_2, CO_2 and CO did not desorb below 375°K the DCOO and DCO intermediates were stable at room temperature where the dissociation steps (2) and (3) were fast. The overall decomposition rate into CO_2 and CO, respectively, was apparently governed by steps (4) and (5) at temperatures up to at least 400°K. The predominate reaction pathway for formic acid decomposition on carburized Ni(110) was the dehydrogenation reaction, steps (2) and (4) above.

The dissociation of adsorbed formic acid into hydrogen and adsorbed formate (DCOO) involved either the recombination of H atoms in step (2a) or the reaction between two adsorbed molecules, step (2b). The shape of the coverage vs exposure curve in Fig. 6 for DCOOH adsorption at 310°K indicated two binding sites were required for dissociation. This observation favors step (2a) as the dissociation step. The failure of the carbide to adsorb H_2 apparently indicated that molecular hydrogen was very weakly bound and the recombination of adsorbed H atoms was rapid even at 200°K. However, the failure to adsorb H_2 may also indicate that the carbide surface was unable to dissociate the hydrogen molecule even though H atoms once formed might be bound. The bulk of the experimental evidence supports the dissociative adsorption of the formic acid molecule.

The dependence of the conversion of DCOOH into DCO and H_2O on exposure indicated that DCO formation was limited to specific sites on the carbide surface which were quickly saturated at low exposure. Figure 6 shows that the amount of CO evolved rapidly increased but leveled off at $3 \pm 1 \times 10^{13}$ molecules/cm^2 after an exposure of only 5×10^{13} molecules/cm^2.

Meanwhile the amount of CO_2 product continued to increase with further exposure. Evidently DCOOH(a) rapidly dissociated at specific sites (σ) into DCO(a) which occupied and quickly saturated these sites. In view of the high probability of CO formation on the clean surface, the specific sites producing DCO(a) on the carbide surface may have been metal sites with few nearby carbon atoms. The observation that the isosteric product distribution remained unchanged with adsorption temperatures from 225 to 325°K further supported the view that the selectivity was determined by dissociation at specific sites and not by parallel reaction steps. Furthermore, if the specific sites were isolated, which seems likely since there were so few relative to carbide sites, then step (3a) would predominate over step (3b), since step (3b) required two adsorbed species to react at an isolated special site to produce four bound species in a single step. Such a complicated reaction appears to be much less likely than the simple fission step of (3a). If this is the case, then either the OH or H fragments must exhibit considerable mobility at room temperature.

The rate of decomposition of the formate intermediate was determined by a reaction step involving the breaking of the D–C or H–C bond. The peak temperature for the β_1-CO_2/DCOOH decomposition was 10°K higher than the peak temperature for HCOO decomposition. A peak temperature shift of this magnitude indicated that the rate had decreased by a factor of two for the deuterated species. The β_2-CO_2 and the CO peaks from DCOOH and HCOOH were not resolved well enough to observe an isotope effect. The β_1-CO_2 isotope effect is discussed further below.

The decomposition of the adsorbed formate, step (4), was not precisely described by two first-order reaction steps from independent binding states, β_1 and β_2. The low temperature side ($T < T_p$) of the β_1 peak and the high temperature side ($T > T_p$) of the β_2 peak were well described by two independent states, but the calculated two-state curve exhibited a dip in the region of overlap between 440 and 470°K as shown in Fig. 8. The dip was removed by adding a third peak with T_p at 435°K,

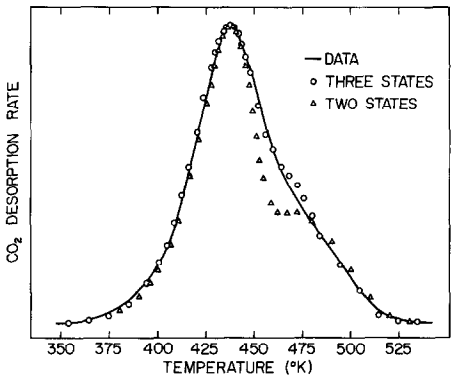

FIG. 8. Formate decomposition on the saturated carbide surface. (—) The CO_2 flash data for HCOOH decomposition following an exposure of 7.2×10^{14} molecules/cm^2. (○) The flash desorption rates calculated from the three-state model; (△) flash desorption rates calculated from the two-state model. The modeled rate was the sum of the desorption rates for two independent first-order binding states. The modeled rates were normalized and shifted along the temperature axis (by less than 15°K) for best comparison with the data.

$$\beta_3\text{-DCOO(a)} \rightarrow \text{D(a)} + \text{CO}_2\text{(g)}. \quad (4')$$

Figure 8 shows the experimental CO_2 desorption curves for HCOOH decomposition with the curves calculated from the two- and the three-state models.

For the three-state model the rate was taken as the sum of the desorption rates for three first-order binding states with

$E(\beta_1) = 25$ kcal/g-mole, $A = 2 \times 10^{12}$ s^{-1};

$E(\beta_2) = 26$ kcal/g-mole, $A = 4.43 \times 10^{11}$ s^{-1};

$E(\beta_3) = 24.5$ kcal/g-mole, $A = 4.0 \times 10^{11}$ s^{-1},

and relative coverages $\beta_1:\beta_2:\beta_3 = 10:$

5:2. For the two-state model the rate was calculated using

$E(\beta_1) = 25$ kcal/g-mole, $A = 2 \times 10^{12}$ s^{-1};

$E(\beta_2) = 15$ kcal/g-mole, $A = 2 \times 10^{6}$ s^{-1},

with relative coverages $\beta_1:\beta_2 = 1:1$. The calculated rates were normalized to the peak maximum and shifted ± 7°K to allow the best curve fit to the total desorption curve.

The desorption rate calculated for just two states fits the gross features of the observed data and by lowering the β_2 state activation energy and frequency factor the magnitude of the dip can be reduced. However, the β_2 peak then becomes very broad and does not adequately fit the high temperature rates or the low coverage decomposition curves. The addition of the β_3 state easily solves this difficulty. In view of the evidence for multiple-site adsorption on the carbide surfaces as discussed previously (*18*), it is concluded that the decomposition of adsorbed formate was best described by three binding states. In any event the addition of the third state does not affect the order of magnitude of the rate parameters describing the β_1 state.

The leading edge of the formate decomposition was easily described by a single (β_1) peak. By fitting a first-order desorption curve to the low temperature side of the β_1-CO_2/HCOOH flash peaks, an activation energy of 25.5 ± 2 kcal/g-mole and a frequency factor of $10^{12.6\pm1}$ s^{-1} were calculated. The rate parameters for both the β_2, β_3 states were within the range: $A = 10^{11\pm1}$ s^{-1} and $E = 25 \pm 1$ kcal/g-mole with a combined maximum coverage of $1.5 \pm 0.5 \times 10^{14}$ molecules/cm^2. This uncertainty in the β_1, β_2, β_3 parameters reflects the reproducibility of the data. In addition, one could probably adjust the β_2, β_3 state parameters over a wider range and still obtain adequate fit to the observed flash curves. The addition of a third state produces three additional parameters, a frequency factor, an activation energy, and a relative coverage, with which to fit the experimental data. The gross features of the dip were eliminated by carefully choosing T_p and the relative coverage. Although T_p was fixed, the frequency factor and activation energy, E, may vary over a few kcal/g-mole (for E) without significantly altering the calculated curve shape. Nevertheless, since the β_2, β_3 state Arrhenius parameters are close to the β_1 state parameters, *the β_1 state shall be considered to qualitatively describe formate decomposition on the saturated carbide surface.*

The frequency factor, $10^{12\pm1}$ s^{-1}, for HCOO decomposition appeared to be a reasonable value consistent with decomposition via breaking the H–C bond. If it is postulated that the formate species is bound by a bond between an oxygen atom and a nickel atom on the surface, then the following decomposition scheme is suggested by the results:

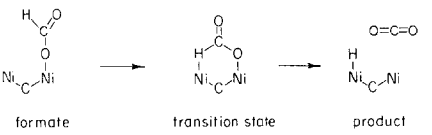

Some entropy (about 6 eu.) may be lost due to the loss of rotation about the O–C bond as the formate species forms the transition state, but the weakened vibrational modes of the Ni–O and H–C bond may partially compensate (about 2 eu.) for this. Thus a frequency factor of about 10^{12} s^{-1} seems reasonable.

Gas phase reactions similar to reaction (4) typically have frequency factors near 10^{13} s^{-1}. The class of gas phase reactions similar to breaking the H–C bond of *adsorbed* HCOO are unimolecular fission reactions, specifically complex fission reactions with four- or five-center cyclic transition states (*23*). Consider the pyrolysis of *n*-PrBr as an example of a four-center complex fission reaction

$$CH_3CH_2CH_2Br \rightarrow C_3H_6 + HBr.$$

The frequency factor observed for this reaction is $10^{13.0}$ s^{-1}; the loss of internal rotation of the CH_3 rotor due to the formation of the double bond was partially offset by the low frequency (and hence high entropy) torsional modes of vibration about the forming double bond. The four-center complex fission reactions typically have frequency factors close to 10^{13} s^{-1}. Table 3.5 of Ref. (*23*) lists 17 four-center fission reactions, all of which have A factors within an order of magnitude of 10^{13} s^{-1}. An example of a five-center complex fission reaction is the pyrolysis of *i*-$PrNO_2$.

$$CH_3CH_2NO_2CH_3 \rightarrow CH_3CH{=}CH_2 + HNO_2.$$

The frequency factor for this reaction is $10^{11.0}$ s^{-1}, a somewhat lower value than $10^{12.0}$ s^{-1}, the estimated A factor (*24*). Here the loss of the NO_2 free rotation about the C–N bond and the loss of CH_3 rotation contributed to the lower frequency factor. In general the frequency factors for gas phase fission reactions involving cyclic transition states fall within the range 10^{11} to 10^{13} s^{-1}, in good agreement with the $10^{12.5 \pm 1}$ s^{-1} frequency factor observed for β_1-HCOO decomposition on the carbide surface. The preexponential factor for simple bond fission reactions are typically much higher (*25*).

The rate of decomposition of DCOO(a) was a factor of two slower than the decomposition of HCOO(a) on both the clean (*26*) and carbide surfaces. The difference in ground state C–H vibrational energy (2900 vs 2160 cm^{-1}) (*27*) is 1.2 kcal/g-mole, favoring the rate of HCOO decomposition by about a factor of four at 400°K. Representing the transition state potential energy surface as a three-dimensional saddle with the reaction coordinate in the Ni . . . H . . . C direction, there are two vibrational modes for the H or D atom perpendicular to the reaction coordinate. These modes are likely to be very low frequency bending modes, and the ratio of the transition state partition functions ($F_D‡/F_H‡$) is then (M_D/M_H), favoring DCOOH decomposition by a factor of two. Thus the net isotope effect of a factor of two favoring HCOOH decomposition is consistent with the postulate that breaking the D–C bond was the rate-limiting step.

The activation energy required to break the C–H bond was not apparently effected by the presence of surface carbon in the carbide form. This is surprising but understandable. Assume that the activation energy for HCOO decomposition was proportional to the difference in the bond energy of an H atom alone on the surface and the surface intermediate, DCOO, i.e., porportional to the energy of reaction ΔE. Then the activation energy would not change if the binding energy for an H atom and a formate species decreased by equal amounts.

C. Chemical Properties of the Carbide Surface

Table 2 summarizes the results for formic acid decomposition over the clean surface (*4,26*) over the carbide surface, over evaporated nickel films (*1,28*) and over silica supported nickel (*29*). The activities observed by Inglis and Taylor (*1*) for Ni films and Fahrenfort *et al.* (*29*) for Ni/SiO_2 were more similar to the results observed for the surface carbide than the clean surface. Inglis and Taylor (*1*) observed $T_r = 455$°K, where T is defined as the temperature where the zero-order decomposition rate was 2.5×10^{15} molecules/cm^2/s. Fahrenfort *et al.* (*29*) observed 468°K with a selectivity, i.e., CO_2/CO ratio of 4.0 (when the product gases were pumped away). The clean Ni(110) surfaces showed $T_r \simeq 390$°K for decomposition of a saturated formate layer whereas $T_r = 455$°K for decomposition of a saturated formate layer on the (4×5) carbide surface. The latter two rates were calculated using $N_{sat} = 0.2 \times 10^{15}$ molecules/cm^2 for the clean and $0.15 \times$

TABLE 2
ACTIVITY AND SELECTIVITY OF SELECTED CATALYSTS FOR FORMIC ACID DECOMPOSITION

Material	E^a	$\log_{10}A^b$	T_r (°K)^d	CO_2/CO	Refs.
Ni(110)	26.6	15.4	390	1.0	(26)
Ni film	15.8	7.9[c]	406	2.7	(30)
Ni film	16.3	7.2[c]	455	2.5	(1)
Ni/SiO_2	23.0	10.2[c]	465	3.2[e]	(31)
Ni foil	20.0	8.5[c]	480	—[f]	(36)
NiC/Ni(110)	25.5	12.5	455	10	This work
Cu powder	26.3	13.1[c]	431	10^4	(35)
Cu film	21.5	10.1[c]	473	1.2	(1)
Cu foil	24.0	10.2[c]	486	~25	(35)

[a] Activation energy (kcal/g-mole).
[b] The zero-order rates (units of 10^{15} molecules/cm^2/s).
[c] Reported in units of molecules/site/s; converted to molecules/cm^2/s by assuming the site density was 1.6×10^{15} site/cm^2.
[d] T_r is defined as the temperature where the rate of decomposition was $10^{14.4}$ molecules/cm^2/s.
[e] Average when product gas was pumped away.
[f] All the CO observed was attributed to reaction at the Pyrex reactor walls.

TABLE 3
ADSORPTION OF CO AND H_2 ON Ni(110), (4 × 5)-C/Ni(110), AND COPPER

Ads./substrate	E^a	$\log_{10}A^b$	N_s^d	S_0	Ref.
CO/Ni(110)	32	16	11	1.0	(26)
CO/Ni-C	21	12.5	11	1.0	(18)
CO/Cu(100)	15	—	9	1.0	(32)
H_2/Ni(110)	23	−1[c]	8	1.0	(4)
H_2/Ni-C	<12	—	Nil	—	(18)
H_2/Cu	8–12	—	Nil	—	(31)

[a] Binding energy (kcal/g-mole).
[b] The first order desorption rates (units of s^{-1}).
[c] In second order units (cm^2/molecule/s).
[d] Maximum coverage for adsorption at 200°K and 10^{-8} Torr (units of 10^{14} molecules/cm^2).

10^{15} molecules/cm^2 (β_1 state) for the carbide surfaces. Walton and Verhoek (28) reported $T_r = 406$°K for decomposition over evaporated nickel films—a value much closer to our results on clean Ni(110). Thus the reaction rates observed by Taylor and Fahrenfort are closer to the reaction rate on (4 × 5)-C Ni(110) than on clean nickel. This observation should be considered cautiously since the activity may differ for different crystal faces.

Levi and Boudart (30) have suggested that transition metal carbides may have chemical properties similar to elements of higher atomic number in the same row of the periodic table. Specifically, the nickel carbide surface may behave more like copper than clean nickel because the *d* band could be filled by the valence electrons of carbon. Although the nature of surface bands may be considerably more complicated than this, comparison of H_2 and CO adsorption on the carbide surface with adsorption on copper as shown in Table 3, offers some support to the chemical effectiveness of this argument. As reported elsewhere (18) hydrogen did not adsorb on the carbide surface, and it is well known that copper does not chemisorb hydrogen at room temperature (31). Also the bonding energy of CO decreased from 32 kcal/mole on the clean Ni(110) surface (26) to about 22 kcal/mole on the carbide surface, whereas Tracy (32) reported 15 kcal/mole average CO bonding energy on Cu(100). The adsorption properties of the nickel carbide surface indeed appear to show a trend toward those of copper.

The activity of the carbide surface for HCOO decomposition also shows similarity with copper. Inglis and Taylor's (1) work on evaporated films showed that a copper film at 473°K (T_r) decomposed formic acid in the zero-order pressure regime at a velocity of 0.16 molecules/site/s with a site density of 1.6×10^{15} sites/cm^2. Tamaru's (33) work on copper powders showed higher activity than the Cu films; T_r for the powders was 431°K. Schwab and Schwab-Agallidis' (34) earlier work on copper foils showed $T_r = 468$°K. These results are included in Table 2 and compare more favorably with the (4 × 5)-C results with $T_r = 455$°K than the clean Ni(110) results with $T_r = 390$°K.

Comparison of the reported activity and selectivity of copper with the above Ni(110) carbide results, should be made cautiously since some of the previous work on nickel films, foils, Ni/SiO_2, etc., also showed better agreement with the carbide results. However, carbon can apparently be removed more readily from a copper surface than from a nickel surface (*32*), and possibly the copper results are indicative of the activity of clean copper. An AES and flash desorption study of formic acid decomposition on clean copper should provide a more meaningful test of the nickel carbide vs copper correlation.

SUMMARY

The carburized surface was two orders of magnitude less active for formic acid decomposition than clean Ni(110). Increasing amounts of surface carbon in the carbide form affected the decomposition by eliminating the very narrow "explosive" CO_2 decomposition characteristic of the clean surface and shifting the decomposition peaks from 390 to 440°K. The selectivity of the Ni(110) surface was dramatically increased by the carbide layer; the CO_2/CO product ratio following saturation HCOOH exposure at room temperature increased from 1.0 on the clean surface to 10 on the (4×5) carbide surface. The production of CO was apparently limited to relatively few specific sites on the carbide surface. This result implies that a uniformly saturated (2×1)-C layer should not dehydrate formic acid.

The decomposition of DCOOH on the carbide surface indicated that the reaction intermediate was DCOO. Following adsorption at 200°K on the (2×1)-C surface, DCOOH produced a broad H_2 flash peak at 290°K and nearly identical D_2 and CO_2 flash peaks at 450°K. The following reaction scheme represents the predominate pathway for flash decomposition following the room temperature exposure of DCOOH to the (2×1)-C surface:

$$\begin{aligned} \text{DCOOH(g)} &\rightarrow \text{DCOO(a)} + \text{H(a)}, \\ 2\text{H(a)} &\rightarrow \text{H}_2\text{(g)} \\ \text{DCOO(a)} &\rightarrow \text{CO}_2\text{(g)} + \text{D(a)}, \\ 2\text{D(a)} &\rightarrow \text{D}_2\text{(g)}. \end{aligned}$$

The decomposition of adsorbed DCOO produced three overlapping D_2 and CO_2 flash peaks. The lower temperature β_1 peak was qualitatively representative of the kinetics of decomposition on the (4×5)-C and (2×1)-C surfaces. The first-order rate constant for the β_1 decomposition peak was $10^{12.5\pm1} \exp(-25.5 \pm 2$ kcal/g-mole$/RT)$ s^{-1}. The frequency factor was much smaller than the corresponding frequency factor of $10^{15.5}$ s^{-1} for formic acid decomposition on the clean Ni(110) surface. Although the activation energies were nearly identical, this indicated that HCOO was less rigidly bound to the carbide surface than to the clean surface or that the transition states for the reaction were substantially different. As on the clean surface, the rate of HCOO decomposition on the carbide surface was twice as fast as DCOO decomposition. An isotope effect of this magnitude was reasonable for a decomposition step involving the D---C bond.

Much of the previous work on nickel catalysts (*2,3*), especially foils and powders, has shown high CO_2 selectivity and low activity for formic acid decomposition, and thus compares more favorably with decomposition on the carburized Ni(110) surface than with decomposition on clean Ni(110). The lowered activity and increased selectivity observed after extended formic acid decomposition on nickel films (*1*) may have been caused by carburization. The loss of superactivity of nickel wires (*5*) after long formic acid exposure at high temperature can be attributed to the formation of surface graphite.

The chemical properties of the carbide layer showed some similarity with copper. The failure of the carbide surface to adsorb hydrogen and the low binding energy

of carbon monoxide correlate well with CO and H_2 adsorption on copper. The reported activity of copper for formic acid decomposition compares more favorably with the activity of the carbide surface than with the activity of clean Ni(110). This evidence is not conclusive, however, since the previously reported activities and selectivities of both copper and nickel varied over a wide range and may be effected by surface carbon or oxygen.

ACKNOWLEDGMENTS

The authors gratefully acknowledge the National Science Foundation and the Center for Materials Research at Stanford for financial support of this research. Acknowledgment is also made to the Donors of The Petroleum Research Fund, administered by the American Chemical Society, for partial support of this research. We are also thankful for fellowship assistance from the National Science Foundation for a portion of this work (J. G. M.). One of us (R. J. M.) is especially appreciative of D. J. Rodine for encouragement in the early stages of this study of the formic acid reaction.

REFERENCES

1. Inglis, H. S., and Taylor, D., *Inorg. Phys. Theor. J. Chem. Soc. A* 2985 (1969).
2. Mars, P., Scholton, J. J. F., and Zweitering, P., *in* "Advances in Catalysis" (D. D. Eley, H. Pines and P. B. Weisz, Eds.), Vol. 14, p. 35. Academic Press, New York, 1963.
3. Bond, G. C., "Catalysis by Metals," pp. 412–432, Academic Press, New York, 1962.
4. McCarty, J. Falconer, J., and Madix, R. J., *J. Catal.* **30,** 235 (1973); also Falconer, J., and Madix, R. J., *Surface Sci.* **46,** 473 (1974).
5. Duell, J. J., and Robertson, A. J. B., *Trans. Faraday Soc.* **57,** 1416 (1961).
6. Robertson, A. J. B., *in* "Chemisorption and Catalysis," pp. 72–79, Inst. Petrol., London, 1970.
7. Coad, J. P, and Rivière, J. C., *Surface Sci.* **25,** 609 (1971).
8. Dalmai-Imelik, G., Berolini, J. C., and Rousseau, J., *Surface Sci.* **27,** 383 (1971).
9. Haas, T. W., Grant, J. T., and Dooley, G. J., *in* "Adsorption-Desorption Phenomena" (F. Ricca, Ed.), pp. 359–368. Academic Press, New York, 1972.
10. Haas, T. W., Grant, J. T., and Dooley, G. J., *J. Appl. Phys.* **43,** 1853 (1972).
11. Ertl, G., *in* "Molecular Processes on Solid Surfaces" (Drauglis, E., Gretz, R. D., and Jaffee, R. I., Eds.), pp. 155–157. McGraw-Hill, New York, 1969.
12. Pitkethly, R. C., *in* "Chemisorption and Catalysis," pp. 107–108, 110–113, Inst. Petrol., London, 1970.
13. Somorjai, G. A., and Farrell, H. H., *Advan. Chem. Phys.* **20,** 282 (1971).
14. Falconer, J., Ph D. dissertation, Chap. 3. Stanford Univ., 1974.
15. Madix, R. J., Falconer, J., and McCarty, J., *J. Catal.* **31,** 316 (1973).
16. Ref. (*14*), App. A.
17. Grant, J. T., and Haas, T. W., *Surface Sci.* **24,** 332 (1971).
18. McCarty, J. M., and Madix, R. J., unpublished data.
19. Madden, H. H., and Ertl, G., *Nederlands Tydschriff voor Vacuumtehniek* **10** (2) (1972).
20. Renshaw, G. D., Roscoe, C., and Walker, P. L., Jr., *J. Catal.* **22,** 394 (1971).
21. Blakely, J. M., Kim, J. S., and Potter, H. C., *J. Appl. Phys.* **41,** 2693 (1970).
22. Shelton, J. C., Patil, H. R., and Blakely, J. M., Materials Science Center Report No. 2036, Cornell Univ., 1973, in press, 1974.
23. Benson, J. W., "Thermonuclear Kinetics," pp. 75–82. Wiley, New York, 1968.
24. Ref. (*23*), p. 79.
25. Ref. (*23*), pp. 69–72.
26. Ref. (*14*), Chap. 4.
27. Tubino, R., and Zerbo, G., *J. Chem. Phys.* **53,** 1428 (1970).
28. Walton, D. K., and Vorhoek, F. H., *in* "Advances in Catalysis" (D. D. Eley, W. G. Frankenburg, V. I., Komarewsky and P. B. Weisz, Eds.), Vol. 9, p. 682. Academic Press, New York, 1957.
29. Fahrenfort, J., Van Reyen, L. L., and Sachtler, W. M. H., *in* "The Mechanism of Heterogeneous Catalysis" (J. H. DeBoer *et al.*, Eds.), Elsevier, Amsterdam, 1960.
30. Levy, R. B., and Boudart, M., *Science* **181,** 547 (1973).
31. Pritchard, J., and Tompkins, F. C., *Trans. Faraday Soc.* **56,** 540 (1960).
32. Tracy, J. C., *J. Chem. Phys.* **56,** 2748 (1972).
33. Tamaru, K., *Trans. Faraday Soc.* **55,** 1191 (1959).
34. Schwab, G. M., and Schwab-Agallidis, E., *Ber. Deut. Chem. Gesel.* **76,** 1228 (1943).
35. Ruka, R. J., Brockway, L. O., and Boggs, J. E., *J. Amer. Chem. Soc.* **81,** 2930 (1959).
36. Popov, A. I., *Chem. NonAqueous Solvents* **3,** 339 (1970).